

Monitoring the Charge-Carrier-Occupied Density of States in Disordered Organic Semiconductors under Nonequilibrium Conditions Using Thermally Stimulated Luminescence Spectroscopy

Andrei Stankevych,^{1,2,‡} Rishabh Saxena^{①,2,‡} Alexander Vakhnin,¹ Falk May,³ Naomi Kinaret,⁴ Denis Andrienko^{①,4} Jan Genoe^{①,5} Heinz Bässler,⁶ Anna Köhler^{①,2,6,*} and Andrey Kadashchuk^{①,2,5,†}

¹*Institute of Physics, National Academy of Sciences of Ukraine, Prospect Nauky 46, 03028 Kyiv, Ukraine*

²*Soft Matter Optoelectronics and Bavarian Polymer Institute (BPS), University of Bayreuth, Universitätsstr. 30, 95448 Bayreuth, Germany*

³*Merck KGaA, Display Solutions department, Frankfurter Straße 250, 64293 Darmstadt, Germany*

⁴*Max Planck Institute for Polymer Research, Polymer Theory department, Ackermannweg 10, 5528 Mainz, Germany*

⁵*IMEC, Sensors and Actuators Technology department, Kapeldreef 75, B-3001 Leuven, Belgium*

⁶*Bayreuth Institute of Macromolecular Research (BIMF), University of Bayreuth, Universitätsstr. 30, 95448 Bayreuth, Germany*

 (Received 9 December 2022; revised 15 March 2023; accepted 23 March 2023; published 2 May 2023)

The dynamics of charge carriers in disordered organic semiconductors is inherently difficult to probe by spectroscopic methods. Thermally stimulated luminescence (TSL) is an approach that detects the luminescence resulting from the recombination of spatially-well-separated geminate charge pairs, usually at low temperature. In this way, the density of states (DOS) for charges can be determined. In this study, we demonstrate that TSL can also be used for probing an occupied density of states formed by a low-temperature energetic relaxation of photogenerated charges. Another approach used to gain an insight into the charge-relaxation process is kinetic Monte Carlo (KMC) simulations. Here, we use both techniques to determine the energetic distribution of charges at low temperatures. We find that the charge dynamics is frustrated, yet this frustration can be overcome in TSL by using an infrared (IR) push pulse, and in KMC simulations by a long simulation time that allows for long-range tunneling. Applying the IR-push TSL to pristine amorphous films of 18 commonly used low-molecular-weight organic light-emitting diode materials, we find that the width of the occupied DOS amounts to about 2/3 of the available DOS. The same result is obtained in KMC simulations that consider spatial correlations between site energies. Without the explicit consideration of energetic correlations, the experimental values cannot be reproduced, which testifies to the importance of spatial correlations for charges.

DOI: [10.1103/PhysRevApplied.19.054007](https://doi.org/10.1103/PhysRevApplied.19.054007)

I. INTRODUCTION

The operation of organic light-emitting diodes (OLEDs) and organic solar cells (OSCs) depends on the motion of charges. A correct description of charge transport is therefore essential if one wishes to model and predict the performance of OLEDs and OSCs. Contemporary modeling approaches include drift-diffusion simulations, kinetic Monte Carlo (KMC) simulations, and master-equation approaches [1–5]. In disordered organic semiconductors, charge transport involves energetic relaxation in a broad

distribution of localized states, usually assumed to be well described by a Gaussian distribution characterized by width σ_{DOS} [6,7]. For thermal equilibrium conditions, this relaxation process is well understood. Charges that are injected or photogenerated at a random energy site in the available density of states (DOS) proceed by a sequence of energetically downward or upward hops to form an occupied density of states (ODOS). This ODOS is placed around an equilibrium energy ($\varepsilon_{\text{eq}} = -\sigma_{\text{DOS}}^2/k_B T$) below the center of the DOS with a width, σ_{ODOS} , equal to the width of the DOS (σ_{DOS}) [6–8].

The active semiconductor layer in typical disordered OLEDs or OSCs is frequently less than 100 nm thick. This implies that charges injected or photogenerated at room temperature in a DOS with $\sigma_{\text{DOS}} \gtrsim 85$ meV do not reach the thermal equilibrium transport regime prior to being

*anna.koehler@uni-bayreuth.de

†kadash@iop.kiev.ua

‡A. Stankevych and R. Saxena contributed equally to this work.

extracted or recombined [9]. The energy and width of the DOS fraction they occupy, i.e., the ODOS, differs from that under equilibrium conditions. Despite its importance for the realistic modeling of charge transport, little is known about the nature of the ODOS under nonequilibrium conditions. This study is concerned with the question of which part of the DOS is visited by charges under nonequilibrium transport.

The ODOS determines charge transport in amorphous organic semiconductor films. Yet, since charges do not emit light, they are difficult to study by direct spectroscopic means, though they can be accessed indirectly. One method to study the energetic relaxation process within the DOS consists of analyzing the decay of the time-of-flight signal. By this approach, the transition from a nondispersive to a dispersive transport regime is empirically found to occur at a critical disorder parameter $(\sigma_{\text{DOS}}/k_B T)_{\text{cr}}$ that depends on the length, L , of the sample, according to $(\sigma_{\text{DOS}}/k_B T)_{\text{cr}}^2 = 44.8 + 6.7 \log_{10} L$, with L being given in cm [6,10].

Furthermore, triplet excitations are used as probe particles to charge transport, as triplets can be monitored spectroscopically and are transported via short-range exchange interactions, similar to charge carriers [6,8,11,12]. There are limitations to this approach. Triplets are neutral unlike charges, and therefore, less susceptible to polarization-induced or dipolar energetic disorder (implying a smaller σ_{DOS}). Triplets are also more localized, so that they are often associated with a stronger distortion of the molecular backbone, and therefore, larger reorganization energy, λ [11]. Furthermore, triplets have a finite lifetime, unlike charges, which have an infinite lifetime if recombination is excluded. Nevertheless, a number of findings can be transferred, at least qualitatively, and triplet energetic relaxation has been extensively studied in the last decades [11–15]. Notably, below a characteristic temperature, the triplet energetic relaxation is found to become not only dispersive, but also progressively frustrated with a further decrease in temperature. Thermally activated jumps that otherwise promote spectral diffusion are frozen out, so that triplets remain kinetically trapped in local energy minima [12].

The nature of the energy landscape of the charge-carrier DOS was studied by Coehoorn and co-workers [16,17]. They analyzed the I - V characteristics in sandwich-type devices based on amorphous small-molecule organic semiconductors, measured for different layer thicknesses and temperatures, and concluded that site energies for charges were spatially correlated in these materials. Thus, it will not suffice to consider only the *width* of the DOS, but the *degree of energetic correlation* also needs to be taken into account, in particular, when describing the observed Poole-Frenkel-type field dependence of charge mobility [16–21].

Here, we employ two approaches to study the relaxation of charge carriers in the nonequilibrium regime. Experimentally, we use the technique of thermally stimulated luminescence (TSL) measurements. TSL is commonly employed to determine the width of the available DOS distribution [22–29]. Here, we advance the method by using an infrared (IR) push pulse that stimulates frustrated charges stuck in intermediate local minima to advance further in the relaxation process, thus accelerating the relaxation process at cryogenic temperatures. With this approach, we investigate 18 common low-molecular-weight OLED materials. The resulting Gaussian distribution of relaxed carriers is found to have a width $\sigma_{\text{TSL}} \approx (2/3)\sigma_{\text{DOS}}$ that we associate with the width of the ODOS in the nonequilibrium regime.

Our second approach consists of simulating the energetic relaxation of charges in the DOS with the kinetic Monte Carlo technique for the two cases of random energetic disorder and spatially correlated site energies [3]. As expected, our simulations confirm $\sigma_{\text{ODOS}} = \sigma_{\text{DOS}}$ for hopping transport at equilibrium. However, for both types of energetic disorder, our simulations also demonstrate that the narrowing of the ODOS is a genuine feature for charge transport in the nonequilibrium regime. In the case of assuming correlated disorder, we obtain $\sigma_{\text{ODOS}} = (2/3)\sigma_{\text{DOS}}$, which matches the experimental value of σ_{TSL} . In contrast, for random disorder, a narrower σ_{ODOS} results.

On the basis of the TSL and KMC results, we conclude that, for amorphous low-molecular-weight organic semiconductor films, a value of $\sigma_{\text{ODOS}} = (2/3)\sigma_{\text{DOS}}$ is representative for the width of the nonequilibrium ODOS at 5 K and that the due consideration of energetic correlation is essential for an accurate quantitative description of charge-carrier relaxation in the DOS.

II. EXPERIMENT

A. Materials

For our study, we use the OLED small organic molecule materials, the chemical structures of which are shown in Fig. 1 along with their abbreviated names. These compounds are purchased from Sigma-Aldrich, Lumtec Taiwan, with the exception of DMAC-py-TRZ, which is provided by Eli Zysman-Colman from the University of St Andrews, UK. Three materials, referred to as HTM-2, ETM-1, and TMM-1, are provided by Merck, and they denote a hole-transport, electron-transport, and triplet-matrix material, respectively. All materials are used as received, without any further purification. Thin films of the above compounds are spin coated from 20 mg/ml chloroform or toluene solutions onto cleaned quartz substrates (1000 rpm, 30 s) that result in typically 50-nm-thick layers. Subsequently, the deposited films are dried in an oven at 40 °C for 10 min and then under vacuum for 2 h to remove residual solvent.

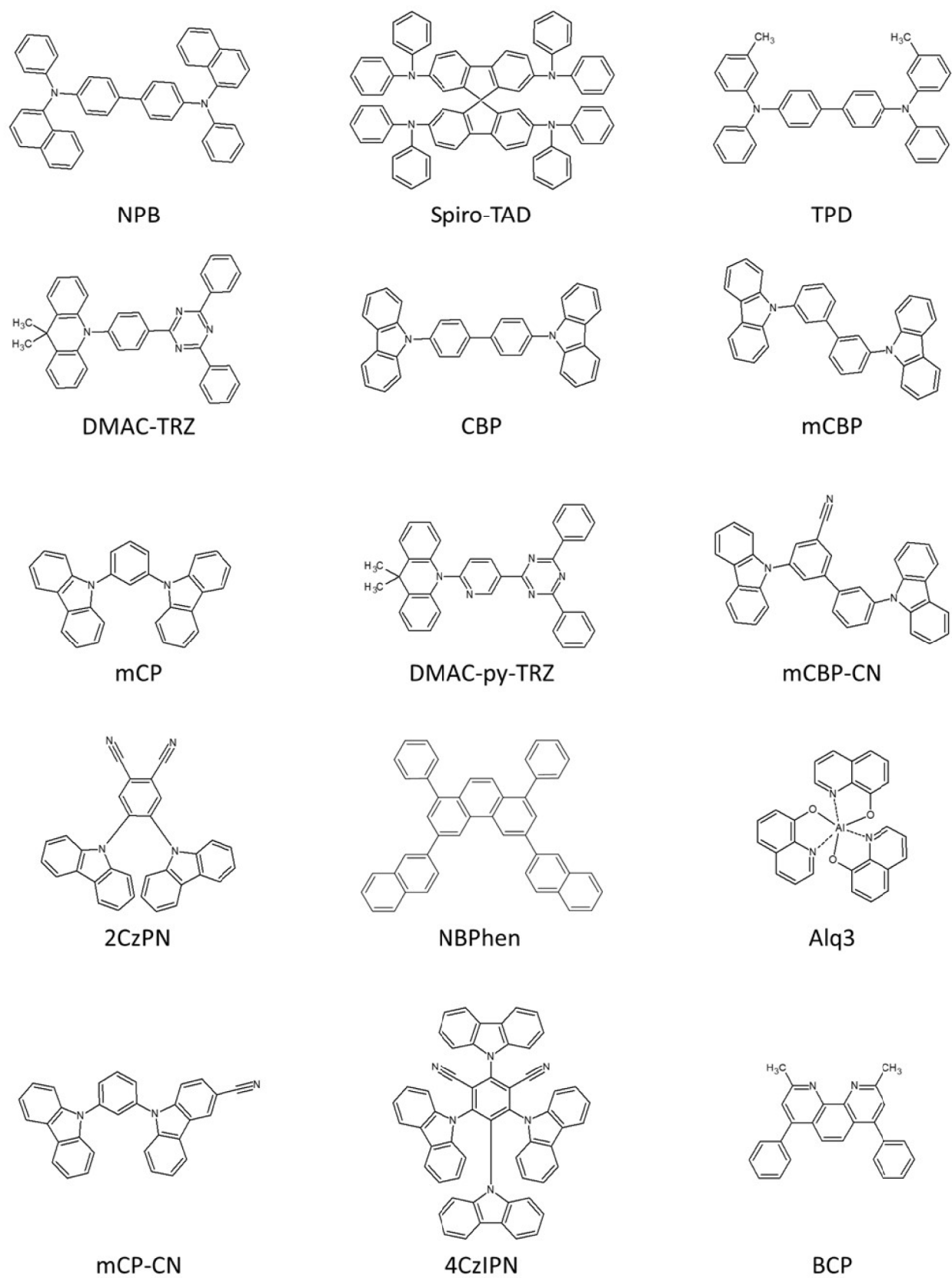


FIG. 1. Molecular structures of the compounds used in this study. Full names are given in Note S1 of the Supplemental Material [30].

B. TSL techniques

TSL is the phenomenon of light emission arising after the removal of excitation (UV light, in our case) under conditions of increasing temperature. Generally, in the TSL method, the trapping states—in the case of pristine amorphous semiconductor films, for example, extrinsic impurity-related traps or the tail states of a DOS distribution—are first populated by the photogenerated charge carriers, usually at low temperatures. After terminating the excitation, the trapped charge carriers can be released by heating the sample, and the luminescence due to charge recombination is recorded as a function of temperature [$I_{\text{TSL}}(T)$]. It is important to note that, in the case of amorphous organic semiconductors, the temperature scale corresponds directly to the activation energy, E_a , for the release of carriers, as detailed further in Note S2 and Fig. S1(b) within the Supplemental Material [30] and also in Refs. [22–27]. For the organic materials studied in the present work, the $\langle E_a \rangle(T)$ dependence, as determined by the fractional (or partial) heating TSL technique [31,32], is found to be described reasonably well by the following empirical relationship [see Fig. S1(b) of the Supplemental Material [30]]:

$$\langle E \rangle(T) = 3.2 \frac{\text{meV}}{\text{K}} \times T - 91 \text{ meV}. \quad (1)$$

TSL measurements are carried out over a temperature range from 5 to 300 K using an optical temperature-regulating helium cryostat. The following text summarizes the methodology adopted for the two different regimes of TSL measurements presented in this study. Please refer to Notes S2 and S3 of the Supplemental Material [30] for a more extensive description of the experiment and its analysis used to determine the width of the available DOS, σ_{DOS} .

1. Classical TSL

In “classical TSL” experiments, samples are cooled to 5 K and excited at 313 nm (cw excitation) for 3 min. The excitation wavelength ($\lambda_{\text{exc}}=313$ nm) is selected from a high-pressure mercury (Hg) lamp spectrum with the help of an appropriate set of cutoff filters. After that, the samples are kept in the dark at a constant temperature (5 K) during a certain dwell time, typically 10–20 min, before the TSL heating run is started to allow the long isothermal afterglow (arising due to isothermal recombination of short-range geminate pairs) to decay to a negligible value. Then, TSL measurements are started upon heating the sample from 5 to 300 K with a linear heating ramp (at a constant heating rate, $\beta=0.15$ K/s). TSL emission (due to the thermally activated recombination of long-range geminate pairs) is detected with a cooled photomultiplier tube operating in photon-counting mode, which is mounted adjacent to the cryostat window. The measured

TSL signals are very weak, typically ranging from several hundred to several thousand counts per second at the TSL peak maximum, depending on the material being measured. Therefore, we are not able to resolve TSL spectrally. However, using glass cutoff filters, we roughly estimate that TSL emission is mostly dominated by the intrinsic phosphorescence of the materials, while a much weaker fluorescence component is also present in TSL.

2. IR-cleansed TSL

After exciting the samples with $\lambda_{\text{exc}}=313$ nm (like in the classical TSL method), samples are additionally irradiated with IR photons for 30 min at 5 K. IR irradiation is selected by using an IR filter with a transparency band of 900–4500 nm from the emission spectrum of the same Hg lamp. It should be noted that no sample heating occurs in the process, and the sample is immersed in liquid helium. After that, the TSL glow curve is recorded upon linear heating, just as in the case of classical TSL. We find that, as a result of such additional IR irradiation (i.e., a long IR-push pulse), the TSL curve acquires a more symmetrical profile. Hereafter, such a procedure is referred to as “*IR cleansing*,” and a possible origin of the effect is discussed in Sec. II C.

C. Experimental results

Figure 2(a) shows the normalized TSL glow curves for a few exemplary organic semiconductor materials, namely, NPB, TPD, mCBP, and NBPhen, obtained under identical conditions using the “classical” TSL technique. The classical TSL glow curve of each material shown in Fig. 2(a) represents a broad band, the position of which on the temperature scale is material specific. In particular, the peak of the TSL glow curve shifts to higher temperatures as the TSL band profile broadens. Upon closer inspection of the TSL band profile, an additional shoulderlike feature becomes evident on the low-temperature side, typically at around 40 K. The relative intensity of this low-temperature component is dependent on the material (in some materials, it is observed as an additional TSL peak). Recalling that the temperature scale corresponds linearly to an activation energy for carrier release, we provisionally ascribe the low-temperature feature to the release of geminate pairs with intermediate distance, e.g., those captured by shallow low-energy sites. On the other hand, there is a possibility that a double-peak TSL curve may also be indicative of the presence of local energetic ordering in an organic film due to spatial energy correlations. As a result, one can imagine two scenarios in which a geminate charge pair might be located either within the same energy-correlated valley (if it is spatially well extended) or the sibling electrons and holes are separated between adjacent valleys. In the first case, TSL primarily probes a greatly reduced local energy disorder within an individual energy-correlated domain,

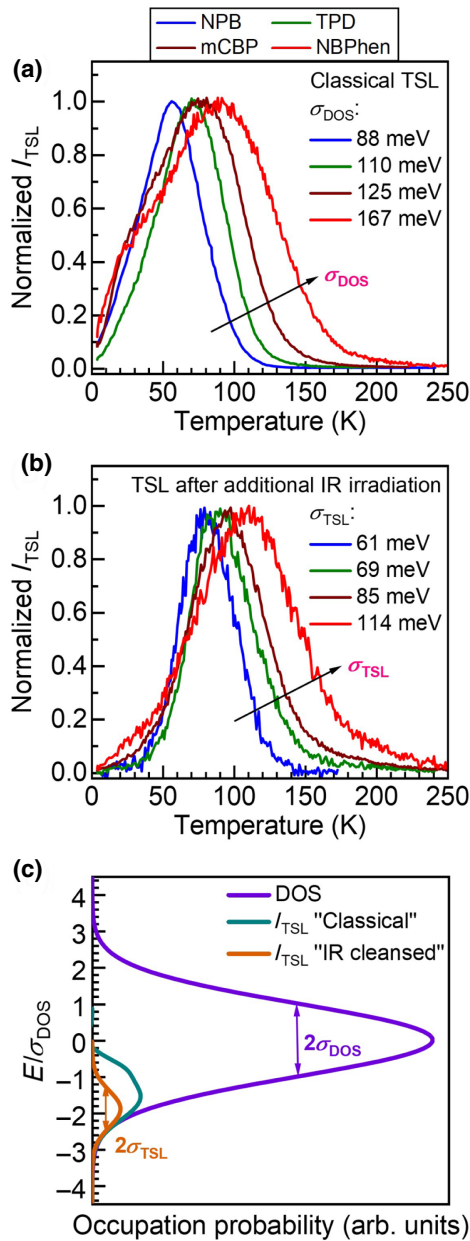


FIG. 2. (a) Normalized TSL intensity (I_{TSL}) curves measured at a constant heating rate of 0.15 K/s after excitation with 313-nm light for 3 min at 5 K in NPB, TPD, mCBP, and NBPhen films. Inset shows σ_{DOS} values obtained by classical TSL. (b) Effect of IR cleansing on the TSL curve profile of NPB, CBP, mCBP, and NBPhen. Inset shows the width of the TSL band, σ_{TSL} , determined for these materials. (c) Schematic illustration of the available DOS distribution (purple curve), classical TSL band formed after low-temperature energy relaxation (dark cyan curve), and TSL band formed after IR cleansing (orange curve). Note that the intensity of the TSL signal, proportional to the occupied density of states, is greatly enlarged for ease of illustration. This is because the concentration of trapped carriers active in TSL is many orders of magnitude smaller than the density of available localized states (DOS) in the system. Therefore, we magnified the TSL signal to demonstrate that its high-temperature part matches the DOS profile.

which results in a very-low-temperature TSL feature. In the latter case, TSL characterizes the distribution of energy barriers between the different energy-correlated valleys, which carriers have to overcome to recombine with their countercharges, and the main TSL peak is therefore relevant to the global energy disorder controlling macroscopic charge transport in a material. This might naturally yield two different TSL peaks. Nevertheless, the precise origin of the low-temperature TSL feature requires further investigation and is beyond the scope of this paper. The key point here is that, by irradiating the sample at 5 K with the 30-min IR-push pulse (IR cleansing), this shoulder-like feature becomes eliminated (effect of IR cleansing), giving rise to a symmetrical TSL peak profile. This is demonstrated in Fig. 2(b). Generally, the IR photons are absorbed by some polaronic states (radical ions) accumulated after the preceding UV excitation, and the absorbed energy is sufficient to release carriers from relatively shallow trapping states active in our TSL measurements. The latter can either recombine with their countercharges or relax towards deeper localized states. A consequence of the additional IR irradiation is that the IR-cleansed TSL peak clearly shifts to a slightly higher temperature, in comparison to the classical TSL, and it is accompanied by a decrease in intensity.

Our interpretation of these data is summarized in Fig. 2(c). In an amorphous thin film, the available density of states can be reasonably well approximated by a Gaussian distribution with standard deviation σ_{DOS} . The low dielectric constant, and consequently, large Coulomb capture radius in the organic materials (for $\epsilon = 3.5$, this radius is as large as 10^3 nm at $T = 5$ K), precludes the generation of free charge carriers upon photoexcitation under the zero-electric-field condition relevant to TSL experiments [7,33]. Therefore, after photogeneration at low temperatures, charge carriers are produced in the form of geminate pairs of opposite charges [33], even if they are loosely bound charge pairs. The separation distance between the charges in photogenerated geminate pairs is subject to distribution. Short-range geminate pairs are rather unstable and recombine by charge tunneling at a constant temperature, giving rise to a delayed fluorescence emission [34–36] and long isothermal afterglow [23]. On the other hand, the long-range geminate pairs can avoid recombination at low temperatures (such as 5 K, relevant to TSL experiments) within a finite time. They relax to low-energy sites in the available DOS, where they shall only be released, and subsequently recombine, upon heating to elevated temperatures. They are therefore responsible for TSL in organic materials, as indicated by the dark cyan curve in Fig. 2(c). Consequently, the high-temperature edge of the TSL glow curve reflects the deep-energy tail of the available DOS, as proven by analytical theory of TSL in a random-hopping system [23,27]. Note, the Coulomb interaction between charges constituting such long-range

geminate pairs is assumed to be insignificant in comparison to the energy disorder in the system, and therefore, is neglected. An analysis of this high-temperature edge, in terms of Gaussian coordinates (see Note S3 of the Supplemental Material [30] for more details), therefore yields the standard deviation of the available DOS, σ_{DOS} , and the values obtained are indicated in Fig. 2(a). The entire band profile of the TSL glow curve itself cannot be analyzed, as it includes the contribution from kinetically trapped intermediate-range geminate pairs. The application of the IR-cleansing long IR-push pulse removes this frustration, so that the charge carriers relax deeply [37,38]. The TSL curve after IR cleansing thus represents the ODOS distribution of the relaxed charge carriers, as illustrated by the orange curve in Fig. 2(c). To estimate the width of the bell-shaped TSL band, (σ_{TSL}), we convert the temperature scale to an energy scale using Eq. (1), as detailed in Note S2 within the Supplemental Material [30]. Then we fit the IR-cleansed TSL curve with a Gaussian function and determine its standard deviation as σ_{TSL} . As discussed further below, we consider that $\sigma_{\text{TSL}} = \sigma_{\text{ODOS}}$.

The approach illustrated in detail for the four compounds of Fig. 2 is subsequently extended to a wider set of materials. Figure 3 shows the IR-cleansed TSL glow curves for all 18 organic materials used in this study, and Table I compares σ_{TSL} derived from the IR-cleansed data and σ_{DOS} parameters obtained from the classical TSL analysis. From such a comparison, we find that σ_{TSL} scales linearly with σ_{DOS} and that the ratio $\sigma_{\text{TSL}}/\sigma_{\text{DOS}} \approx 2/3$. Surprisingly, this turns out to be a general effect for all amorphous organic semiconductor films we measure so far, with a mean value of $\sigma_{\text{TSL}}/\sigma_{\text{DOS}} = 0.64 \pm 0.04$. For comparison, computed σ_{DOS} values, as obtained from quantum mechanics (QM) and molecular mechanics (MM) molecular dynamics simulations [22,28,30,39,40] are also listed in Table I. The DOS width (σ_{DOS}) obtained from classical TSL measurements are in reasonable quantitative agreement with the computed σ_{DOS} . This proves that energetic disorder values observed experimentally, including the large energetic disorder ranging from $\sigma_{\text{DOS}} = 125$ to above 200 meV (Table I), characterize the intrinsic DOS, i.e., the DOS of a chemically pure disordered material, rather than that affected by impurity-related traps.

A noteworthy observation is that for all compounds, except HTM-2, σ_{DOS} exceeds the value of 85 meV, above which charge transport in 100-nm-thick films will not reach equilibrium at room temperature prior to extraction [6,10]. Thus, the nonequilibrium ODOS deserves consideration for the description of transport in corresponding devices. Furthermore, there are two important consequences of the finding that $\sigma_{\text{TSL}}/\sigma_{\text{DOS}} \approx 2/3$. (i) From a practical perspective, this suggests a useful methodology for determining the DOS width. Experimentally, it is straightforward to estimate σ_{TSL} by Gaussian fitting of the whole TSL curve (“ODOS assessment”) measured after

IR cleansing, and then to account for the factor 2/3 for obtaining σ_{DOS} . (ii) From a fundamental point of view, the observed ratio of $\sigma_{\text{TSL}}/\sigma_{\text{DOS}} \approx 2/3$ implies a kind of “spectral-narrowing” effect occurring for the ODOS at low temperatures. This experimental finding obviously requires a theoretical justification. Therefore, we further carry out a KMC-simulation-based study to gain a deeper insight into charge-carrier energetic relaxation phenomena at low temperatures.

III. KINETIC MONTE CARLO SIMULATIONS

A. Simulation techniques

The energetic relaxation of charges in a disordered organic solid is studied by using a grid-based KMC simulation method to monitor the motion of charge carriers as hopping events. The KMC simulations are done by employing an isotropic three-dimensional simulation box ($100 \times 100 \times 100$ lattice sites) with a lattice constant of $a = 1.5$ nm [41,42]. We consider both random- and spatially correlated energetic disorder. For the simulations with uncorrelated disorder, the lattice sites are assigned a random energy drawn from a Gaussian distribution $g(\varepsilon)$ with a standard deviation σ_{DOS} centered at zero energy:

$$g(\varepsilon) = \frac{N}{\sigma\sqrt{2\pi}} \exp\left[-\frac{1}{2}\left(\frac{\varepsilon}{\sigma_{\text{DOS}}}\right)^2\right]. \quad (2)$$

For systems with correlated disorder, the energy correlations between the lattice sites are modeled using the approach suggested by Bobbert and co-workers [3]. The energy at site i is taken to be equal to the electrostatic energy resulting from permanent random dipoles, \vec{d}_j , of equal magnitude, d , but with random orientations on all the other organic sites, $j \neq i$. The resulting DOS is a Gaussian, with a width, σ_{DOS} , proportional to d [19]. The on-site energy, E_i , is then evaluated by using the Ewald summation method:

$$E_i = - \sum_{j \neq i} \frac{e\vec{d}_j(\vec{r}_j - \vec{r}_i)}{\varepsilon_0\varepsilon_r|\vec{r}_j - \vec{r}_i|^3}, \quad (3)$$

with the sum over all sites j in a large cubic box of 30 lattice sites (in each direction) around site i ; e is the unit charge, ε_0 is the vacuum permittivity, and ε_r is the material’s relative permittivity. As pointed out by Bobbert and co-workers [3], with increasing the dimension of the box used for calculating the sum in Eq. (3), charge-dipole interactions can be considered in a progressively accurate manner. In this study, to obtain a fair compromise between accuracy and computation time, we take the sum over all sites j in a large cubic box of 30 lattice sites (in each direction) around site i . In this study, we take $\varepsilon_r = 3$ for all simulations. The resulting disorder strength is then given by

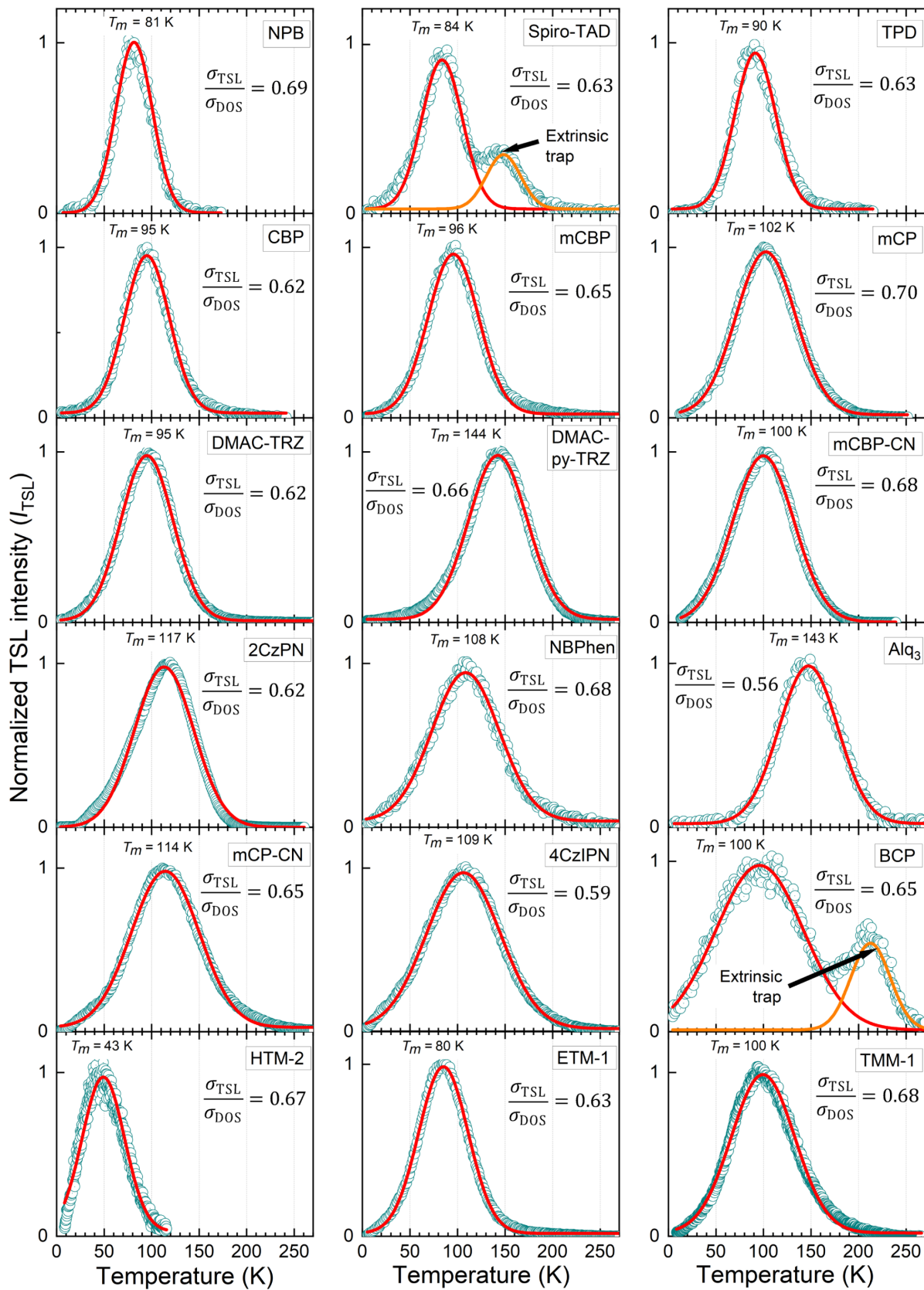


FIG. 3. TSL curves of different organic semiconductor films obtained after IR cleansing. Experimental data are shown by symbols, and solid lines are the fitted Gaussians.

TABLE I. Comparison between the DOS width (σ_{DOS}), energy width of the TSL peak (σ_{TSL}), and the $\sigma_{\text{TSL}}/\sigma_{\text{DOS}}$ ratio for a set of amorphous organic semiconductors. The last column shows the theoretical σ_{DOS} parameter derived from QM-MM calculations.

	Material	σ_{DOS} (meV)	σ_{TSL} (meV)	$\sigma_{\text{TSL}}/\sigma_{\text{DOS}}$	Theoretical σ_{DOS} (meV)
1	NPB	88	61	0.69	87 [28]
2	Spiro-TAD	110	69	0.63	90 [28]
3	TPD	110	69	0.63	—
4	DMAC-TRZ	110	66	0.60	129 ^a
5	CBP	125	77	0.62	100 [22]
6	mCBP	131	85	0.65	122 [28]
7	mCP	140	99	0.70	160 [28], 157 [39]
8	DMAC-py-TRZ	151	99	0.66	—
9	mCBP-CN	151	102	0.68	200 [22]
10	2CzPN	161	100	0.62	—
11	NBPhen	167	114	0.68	194 [28]
12	Alq3	177	99	0.56	150 [40]
13	mCP-CN	177	115	0.65	240 [22]
14	4CzIPN	213	125	0.59	220 ^a
15	BCP	226	147	0.65	190 [28]
16	HTM-2	73	49	0.67	79 ^a
17	ETM-1	103	65	0.63	127 ^a
18	TMM-1	132	90	0.68	140 ^a
Mean				0.64 ± 0.04	

^aSee the Appendix for a theoretical method of σ_{DOS} computation.

$\sigma_{\text{DOS}} \approx 2.35(ed/\varepsilon_r\varepsilon_0a^2)$. Figures 4(a) and 4(b) illustrate the impact of spatial correlations on the energy landscape in an arbitrary X - Y plane (two-dimensional cross section) of the simulation box. In the case of a system with random disorder [Fig. 4(a)], the position of energetic peaks and valleys is found to be completely uncorrelated. On the contrary, in the case of a system with correlated disorder, the sites of higher (lower) energy depicted with blue (red) color [Fig. 4(b)] are found to be in the vicinity of other higher (lower) energy sites. The spatial correlation function, $C(r_{ij})$, which quantifies the degree of correlation between sites at a separation of r_{ij} from each other can be expressed as

$$C(r_{ij}) = \frac{\langle (E_i - \langle E \rangle) (E_j - \langle E \rangle) \rangle}{\langle (E_i - \langle E \rangle)^2 \rangle}, \quad (4)$$

where E_i and E_j are the energies of sites i and j separated by a distance r_{ij} , and $\langle \dots \rangle$ represents the expectation value. $C(r_{ij})$ is 1 if E_i and E_j are fully correlated and 0 if they are uncorrelated. The spatial correlation function evaluated for the energy sites of the X - Y plane in Figs. 4(a) and 4(b) is shown in Figs. 4(c) and 4(d), respectively. While $C(r_{ij})$ is found to be 0 for the system with random disorder, it exhibits a $1/r_{ij}$ dependence for the system with randomly oriented site dipoles, as expected from the interaction of a charge with the long-range-dipole electrostatic potential of a three-dimensional ensemble of uncorrelated dipoles [19].

Hopping transitions in our system are described using Miller-Abrahams hopping rates between an initial site of

energy ε_i and a final site of energy ε_j :

$$W_{ij} = \nu_0 \exp(-2\gamma R_{ij}) \exp\left[-\frac{|\varepsilon_j - \varepsilon_i| + (\varepsilon_j - \varepsilon_i)}{2k_B T}\right], \quad (5)$$

where R_{ij} is the hopping distance and γ is the inverse localization radius. ν_0 is the attempt-to-escape frequency, which is usually close to an intermolecular phonon frequency; k_B is the Boltzmann constant; and T is temperature. The parameter γ is assumed to be isotropic in all directions. Unless otherwise specified, γ is chosen as 2 nm^{-1} (such that $2\gamma a = 6$), as this value is a representative value commonly utilized in theoretical modeling of hopping-charge transport in amorphous organic semiconductors. To consider transitions of carriers to non-nearest hopping sites, we implement variable-range hopping in the KMC simulations by allowing long-distance jumps up to the tenth-nearest neighbor. The probabilities of such jumps are determined by the carrier localization parameter ($2\gamma a$).

Furthermore, both variable-time-step (VT) KMC and constant-time-step (CT) KMC approaches are utilized to solve the master equation. For VT KMC simulations, the following procedure is employed. At the beginning of the simulation, $t = 0$, a charge carrier is generated randomly at one of the lattice sites. At each kinetic step, the charge can hop to any of the nearest-neighbor sites. In the case of KMC simulations in the VRH regime, a charge carrier is also allowed to access non-nearest hopping sites. Every permissible hop is treated as an event, and for each event,

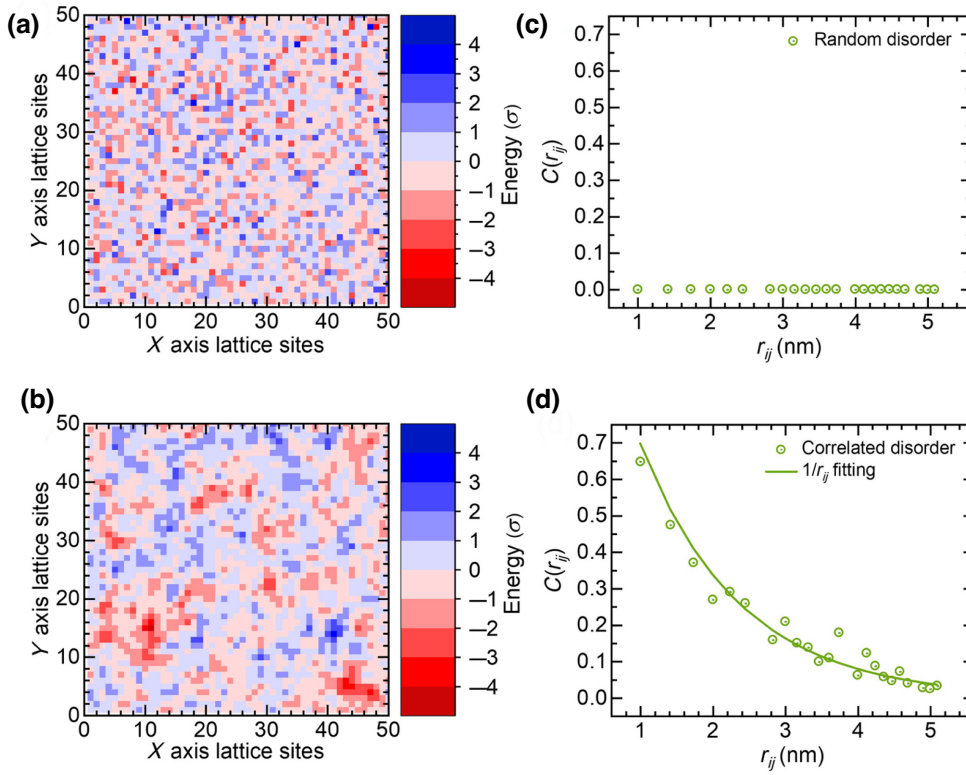


FIG. 4. Heatmap of energetic landscape for a system with (a) random disorder and (b) correlated disorder. Variation of spatial energy correlation function, $C(r_{ij})$ [see Eq. (4)] with distance for (c) random disorder system and (d) correlated disorder system.

i , the rate, W_i , is calculated. For the selection of an event, first, for each event i , the partial sum, $S_i = \sum_{j=1}^i W_{ij}$, is calculated. A random number, φ , is drawn from the interval $(0, 1]$ and from all possible events; the event i for which $S_{i-1} < \varphi W_T \leq S_i$ holds is selected, with $W_T = \sum_{j=1}^{N_{\text{tot}}} W_{ij}$ and N_{tot} being the total number of events (permissible hops). The selected event is executed and the simulation time (t) is updated by the waiting time, $\tau_w = -\ln(X)/W_T$, where X is a random number between 0 and 1.

In the CT KMC simulations, total number of hopping neighbors, N_{tot} , is defined within a cube consisting of $5 \times 5 \times 5$ lattice sites. A hopping event from state i to a generic state j ($i \neq j$) is sampled uniformly from $N_{j \dots \text{tot}}$ hopping neighbors, and rate W_{ij} is calculated. The event is accepted if the associated hopping probability $f_{ij} = (W_{ij}/v_0) > n$, where n is a uniform number between 0 and 1, and v_0 is the rate in a lattice without disorder. Simulation time (t) is updated by $\Delta t = (1/v_0 N_{\text{tot}}) \ln(1/X)$, where X is a random number, such that $X \in (0, 1]$. If the event is accepted, event $i \rightarrow j$ is executed and charge-carrier coordinates are updated. The timescale is defined by $t_0 = 1/(v_0 N_{\text{tot}})$.

Here, the CT KMC simulation method is used to gain an insight into the charge-carrier energy relaxation in short and intermediate time regimes. As the charge carriers relax within the DOS, the hopping rates, W_{ij} (and W_T), can decrease abruptly (by orders of magnitude), even if the number of hopping sites remains constant. Thus, the majority of CT KMC simulation trials are rejected, leading

to computationally intensive simulations. On the other hand, in VT KMC simulations, the time step is evaluated as the inverse of W_T , which leads to a nonlinear increase in the time step as the charge carriers relax in energy. As a result, we lose temporal resolution, and hence, the VT KMC simulation results will be parametrized in terms of the number of hops. However, this allows us to examine the long-time limit of the charge-carrier relaxation process at a reasonable computational cost using the VT KMC simulation method.

B. Simulation results

As mentioned in Sec. II, the TSL curve itself is expected to map a distribution of charge carriers localized within the lower-energy states of the DOS distribution, i.e., the ODOS distribution, formed because of the downward hopping of charges within the DOS at 5 K. For comparison with the TSL experiments, we are therefore interested in the long-time limit of the energetic relaxation of the charges, and hence, we consider VT KMC simulation results. The selected simulation temperature ($T = 5$ K) corresponds to a “nonactivated relaxation” mode [10], often termed the regime of purely downward hopping motion. In contrast, at a moderate degree of disorder (and high enough temperature), charge carriers enter the regime of “activated relaxation” after a critical time (known as the segregation time) [14]. As in previous theoretical studies of

low-temperature energy relaxation and TSL in a random-hopping system [23,27], we assume a very weak interaction between charges within long-range loosely bound geminate pairs responsible for TSL, and therefore, disregard the Coulomb contribution to the difference in energies of neighboring localized sites and to the jump rate. Thus, the energy-relaxation process in TSL is treated the same as that for noninteracting charge carriers.

The evolution of the distribution of charge carriers in a system with random disorder of the DOS width, $\sigma_{\text{DOS}} = 50$ meV, is depicted in Fig. 5(a). Data illustrated are the Gaussian fit results of the energy distribution of charges obtained after a certain number of hops. As shown and discussed further below [see also Fig. S3(a) within the Supplemental Material [30]], the actual distribution of occupied sites after a few hops is not fully symmetric. While the low-energy part, being limited by the number of available neighbors, follows the Gaussian distribution, the high-energy part falls off more steeply. The Gaussian fits to the overall shape are, however, sufficient to capture the general features of the evolution.

In particular, we observe that, with an increasing number of hops, the energy distribution of charges moves to deeper localized states and narrows. The mean energy ($\langle \varepsilon \rangle$) and width (σ) of the charge-carrier ensemble, both normalized by the DOS width (σ_{DOS}), are plotted in Fig. 5(b) as a function of number of hops. A significant initial drop in the mean energy is observed, followed by a decrease in the relaxation rate. The largest shift in mean energy

($\langle \varepsilon \rangle \approx -2.5 \sigma_{\text{DOS}}$) is observed within the first 20 hops [Figs. 5(a) and 5(b)]. This is because only the newly visited sites contribute to the shift in the mean energy, $\langle \varepsilon \rangle$ [8,14,43], and as the charges relax to deeper localized states, the availability of suitable energy sites decreases. In other words, once a charge is captured by a deep trap, it oscillates infinitely and never leaves the local minima. This feature is also captured in the VT KMC simulations. As shown further in Fig. S2 within the Supplemental Material [30], the number of newly visited sites increases significantly within the first 20 hops followed by a slow increase for a higher number of hops. It is to be noted that even after 10^6 hops the number of newly visited sites remains less than 10, in agreement with previous reports [8,14,43].

Analogous to the evolution of the mean energy, a considerable initial narrowing of the energy distribution of the charges is followed by an almost constant σ as the number of hops is increased further. Since dynamic equilibrium is unattainable at 5 K, the charge packet evolves infinitely with simulation time. However, a further increase in simulation time should not drastically affect the distribution of charges oscillating in the vicinity of local minima, and hence, the charge ensemble after 10^6 hops can be considered as the ODOS distribution of the charges. We are particularly interested in the distribution of the ODOS.

In the original Gaussian disorder model (GDM) [6], any spatial correlations between the energies of the hopping sites are disregarded. The inclusion of correlations between the energies of adjacent sites in the correlated disorder

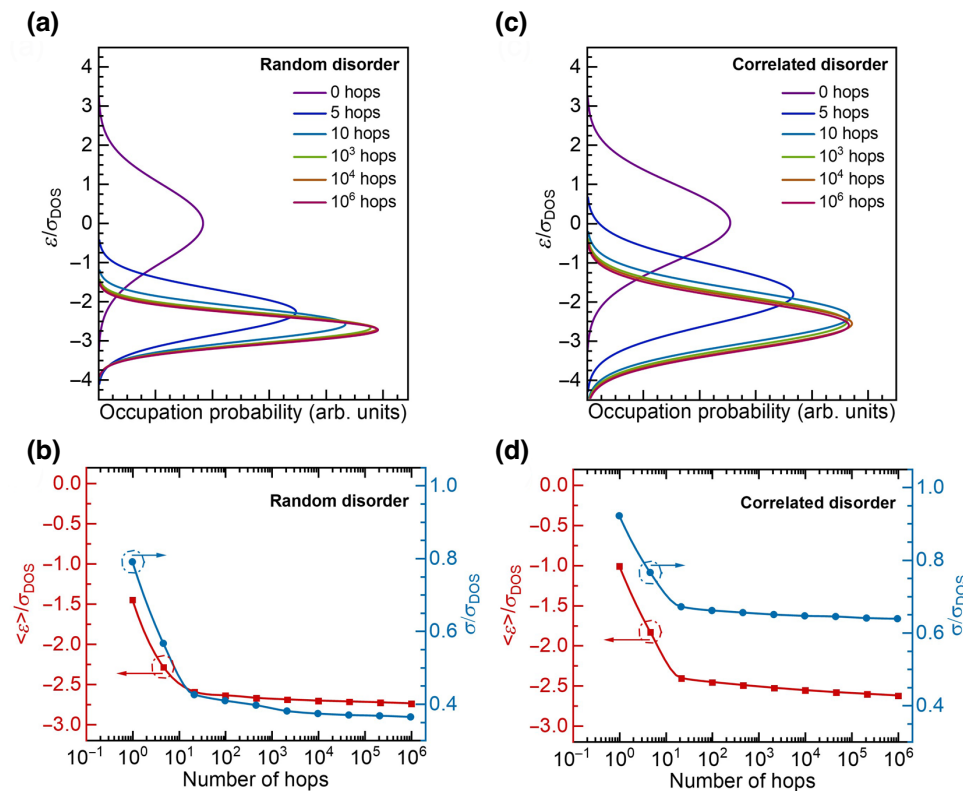


FIG. 5. VT KMC simulation results. Evolution of charge distribution with the number of hops for a system with (a) random and (c) spatially correlated energetic disorder. Data illustrated are Gaussian fit results of the energy distribution of charges obtained after the specified number of hops at 5 K. Variation of mean energy ($\langle \varepsilon \rangle$) and width (σ) of the charge-energy distribution (both normalized by the DOS width, σ_{DOS}) with the number of hops for (b) random and (d) correlated disorder.

model is crucial in predicting the Poole-Frenkel mobility field dependence over a broad field range [16–19,21]; however, the impact of correlation has never been considered in the context of the energetic relaxation of charges. Since the materials used in this study are polar materials [22,28,44] and the TSL measurements are performed at zero fields, we now turn our attention to the results obtained for charge-carrier relaxation in an energy-correlated medium. Like the system with random energetic disorder [Fig. 5(a)], the charge ensemble shifts to lower energy and narrows in the case of correlated disorder system as well [Fig. 5(c)]. However, unlike the uncorrelated disorder system, the narrowing effect is considerably weaker in the system with spatially correlated disorder. We surmise that for random disorder all hops to the new sites dominantly contribute to narrowing; in contrast, hops among correlated sites with almost the same energies cause only limited energy loss. It can be seen from Fig. 5(d) that, within the span of the first 20 hops, the width of the energy distribution of the charges reduces to $0.42 \sigma_{\text{DOS}}$ for random disorder versus $0.67 \sigma_{\text{DOS}}$ for correlated disorder, leading eventually to a larger ODOS width of $\sigma_{\text{ODOS}} = 0.64 \times \sigma_{\text{DOS}}$ [Fig. S3(b) in the Supplemental Material [30]]. $\langle \varepsilon \rangle$ is set to 0 prior to the first hop. It decreases significantly within the course of first 20 hops followed by a slow logarithmic dependence on the number of hops [Fig. 5(d)]. The shift in mean energy after 10^6 hops is almost equal for the systems with correlated ($\langle \varepsilon \rangle \approx -2.6 \sigma_{\text{DOS}}$) or random disorder ($\langle \varepsilon \rangle \approx -2.7 \sigma_{\text{DOS}}$). In general, the nonactivated relaxation of carriers clearly takes place at such low temperatures and the average rate of distribution narrowing decreases with increasing number of hops. Accounting for the spatial energy correlations, which are indeed present

in organic media, allows experimentally obtained values for the ODOS width to be reproduced, i.e., the calculated σ_{ODOS} in a correlated system is approximately equal to σ_{TSL} evaluated experimentally.

Finally, it is worth mentioning that the ratio of $\sigma_{\text{ODOS}}/\sigma_{\text{DOS}} = 0.64$ obtained for correlated disorder shows virtually no dependence on either dielectric permittivity, ε_r , or the amount of dipolar disorder ranging from 50 to 150 meV, implying that the effect does not depend on the polarity of the materials and the DOS width. We observe a very small impact of the $2\gamma a$ factor, varied between 1.5 and 12, on the above ratio. On the other hand, since the lattice constant, a , and the inverse localization radius, γ , are not expected to differ significantly for the low-molecular-weight materials considered herein, it is therefore not surprising that the experimentally obtained 2/3 ratio is common to all of them.

1. Temperature and time dependence

So far, we focus on the nonactivated relaxation process, i.e., carrier jumps can only take place to lower-energy sites. We next take thermal activation into account for both a system with random disorder and with correlated disorder ($\sigma_{\text{DOS}} = 50$ meV), as shown in Figs. 6(a) and 6(b), respectively. We use the CT KMC simulation approach to obtain a dependence in the hopping time rather than in the number of hops. This allows for precise temporal tracking of charge-carrier relaxation.

A significant drop of mean energy is observed for $t < 10^4 t_0$, indicating fast initial energy dissipation for all simulated temperatures. This is followed by a slower dissipation process at longer times. A particular notable feature of

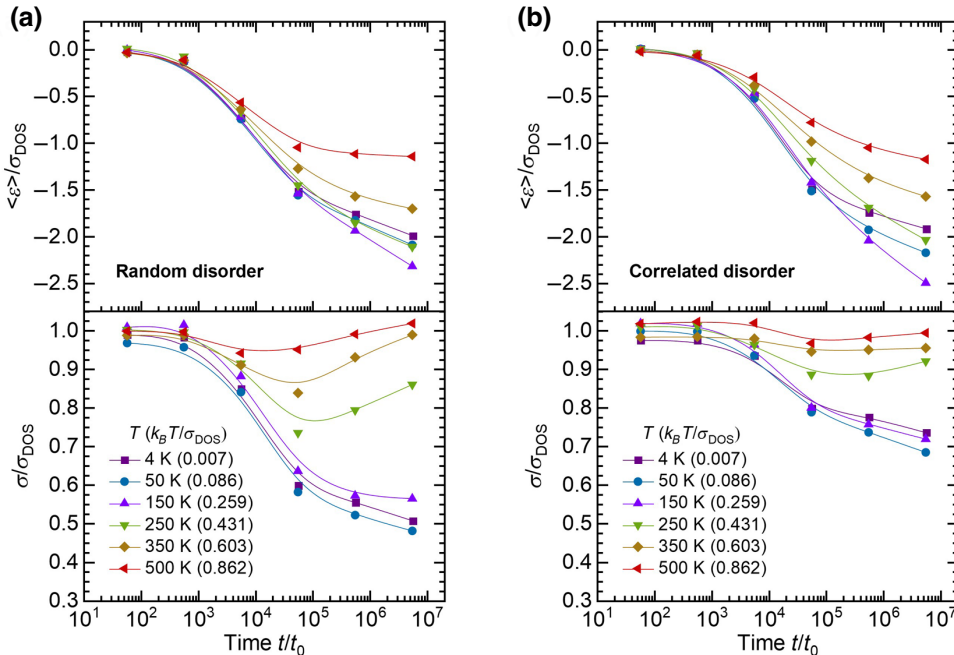


FIG. 6. CT KMC simulation results. Simulated normalized variation of mean energy ($\langle \varepsilon \rangle / \sigma_{\text{DOS}}$, top panels) and the energetic width ($\sigma / \sigma_{\text{DOS}}$, bottom panels) of the distribution of charges as a function of simulation time at variable temperatures for a system with (a) random disorder and (b) correlated disorder. Results are shown for CT KMC simulations performed for a DOS distribution of width $\sigma_{\text{DOS}} = 50$ meV. Solid lines serve as a guide to the eye.

the temperature dependence of charge-carrier relaxation is that the mean energy (at $t = 10^7 t_0$) decreases upon cooling from 500 to 150 K but then increases when the temperature is further reduced to 4 K. This phenomenon can be explained by the concept of frustrated spectral diffusion. The key idea is the following. The charges relax in the DOS by executing jumps to neighboring sites. These jumps may be downhill in energy or uphill, provided there is sufficient thermal energy for uphill jumps. As the temperature reduces, uphill jumps become less likely and are eventually frozen out. However, to get to lower-energy sites via nearest-neighbor-jumps, occasional uphill jumps may be required. Their freezing out can therefore frustrate the overall relaxation process, so that the carriers remain in a local energy minimum. The occurrence of this frustrated spectral diffusion is observed experimentally for triplet excitations [11]. KMC simulations by Athanasopoulos *et al.* demonstrate that frustration can be lifted if more neighboring sites are available or if jumps can occur to sites further away [12]. The top panels of Figs. 6(a) and 6(b) thus illustrate the impact that falling out of thermal equilibrium—here below 150 K (corresponding to $k_B T / \sigma_{\text{DOS}} < 0.26$)—has on the mean energy of the charges. The bottom panels of Figs. 6(a) and 6(b) focus on the effect of energy relaxation on the ODOS width. For $t < 10^4 t_0$, the width reduces with increasing time. At longer times, this reduction continues for temperatures below 150 K. In contrast, for higher temperatures, the width increases as time proceeds. This effect occurs in a similar manner for both random and correlated disorder, yet the overall reduction of the width is significantly reduced when correlated disorder is considered.

IV. DISCUSSION AND CONCLUSIONS

In amorphous organic semiconductor films, energetic relaxation of excitations occurs by a sequence of random hops. The condition of finding a low-energy hopping site is easily met in the center of the DOS, so that downhill hops are fast. Yet, for the hopping sites in the tail of the DOS, suitable hopping sites are further apart, which slows down the transfer. As a result, the excitations generated in the center (or high-energy part) of the DOS distribution relax faster than the ones generated in the tail of the DOS. Figure 7(a) demonstrates the temporal evolution of the energy distribution of the charge carriers generated uniformly over the DOS at high temperatures (T) and/or low σ_{DOS} , i.e., in the regime of equilibrium transport. The distribution shows some narrowing at *earlier times* because of the domination of downwards hops in such a time domain. However, as time progresses, the carrier distribution starts to broaden, as the carriers in lower part of the DOS start relaxing at later times via executing upward hops. Such a nonmonotonous temporal evolution of relaxed

carrier distributions [Fig. 7(a)] is obtained because the carrier's capture by local energetic minima is much faster than its release. Eventually, thermal equilibrium is established, and ODOS is formed around the equilibrium energy ($\varepsilon_{\text{eq}} = -\sigma_{\text{DOS}}^2 / k_B T$) with a width, σ_{ODOS} , equal to the width of the DOS (σ_{DOS}) [6]. On the contrary, at low temperatures, and consequently in the regime of nonequilibrium dispersive transport ($\sigma_{\text{DOS}} / k_B T \gg 1$; high σ_{DOS} or low T), the thermal equilibrium is unattainable. Therefore, at low temperatures, the photogenerated excitations hop towards the lower-energy sites until they reach the DOS tail [Fig. 7(b)]. At any instance in time, irrespective of the mean energy of the relaxed charge-carrier ensemble, the excitations at relatively higher-energy sites within the DOS still relax faster than the excitations at relatively deeper energy sites. As a result, the width (σ_{ODOS}) of the relaxed charge-carrier ensemble decreases monotonously with increasing time [Fig. 7(b)]. These two scenarios are well reproduced in the CT KMC simulation results presented in Fig. 6, which clearly demonstrate that ODOS narrowing is a consequence of nonequilibrium transport. This is also corroborated by previous reports, which suggest that in the regime of equilibrium transport such a narrowing is absent [6,14]. The observation that an ODOS smaller than the full DOS width is a result of the nonequilibrium nature of the transport has not been made before. It is a significant result of our study.

As briefly mentioned in Secs. I and III, the energetic relaxation has already been extensively studied for singlet and triplet excitations and is manifested as spectral diffusion in this context [45]. Experimentally, spectral diffusion is visualized as the bathochromic shift of fluorescence and phosphorescence with temperature for many conjugated systems, such as poly(*p*-phenylenevinylene) [46], poly(*p*-phenylene) [11–13], and polyfluorenes [12,47], as well as for small-molecule materials, such as thermally activated delayed fluorescence emitters [48] and dendrimers [49]. It is also crucial in analyzing the photocurrent and photoluminescence spectra of charge-transfer states in donor-acceptor blends, commonly used as an active layer in organic solar cells [50–53]. Although a lot of attention is given to the shift in the mean energy of the relaxed excitation ensemble as spectral diffusion progresses, spectral narrowing is often not analyzed nor discussed [12,47]. Recently, Kahle *et al.* [54] pointed out that the experimentally observed fluorescence linewidths were significantly lower than those of absorption. This implies that the radiative decay of excitations occurs before spectral diffusion attains equilibrium, and thus, further illustrates the importance of spectral narrowing studies in the regime of nonequilibrium transport.

While the migration of singlet and triplet excitations can be examined spectroscopically, it is difficult to monitor the diffusion of charges. Though the charge-carrier relaxation dynamics process cannot be probed with TSL,

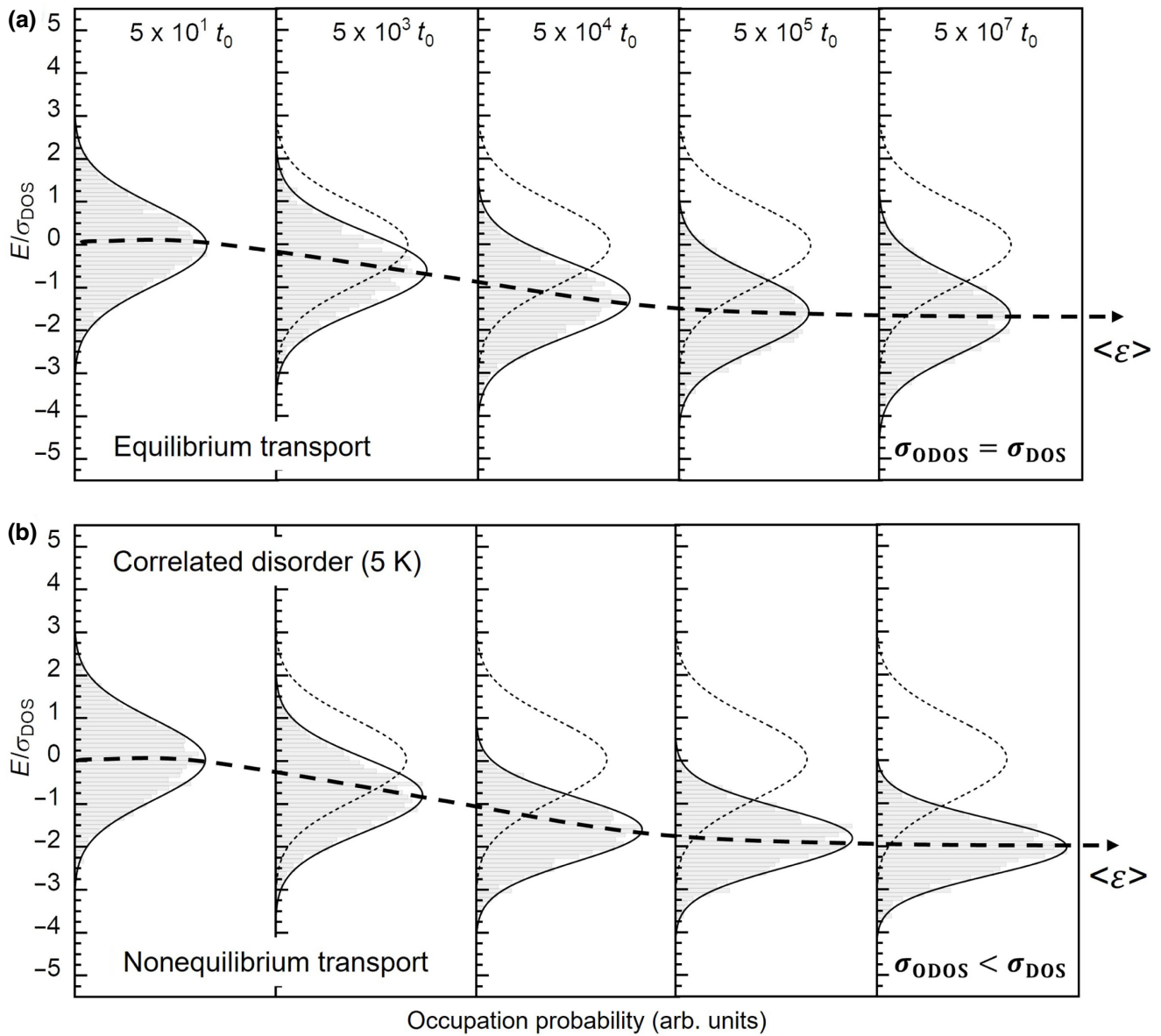


FIG. 7. Schematic representation of the temporal evolution of the charge-carrier ensemble for (a) equilibrium transport (b) nonequilibrium transport for selected time intervals. Initial distribution is indicated throughout by the dotted line for reference.

the latter technique allows us to investigate the ODOS distribution formed as a result of the charge-carrier relaxation process. As shown in the KMC simulation results of Figs. 5 and 6, relaxation never achieves equilibrium at low temperatures. Although the rate of relaxation is fast at earlier times, it slows down as time progresses. At long delay times after excitation, the mean energy and energetic width of the charge-carrier ensemble virtually saturates. It is therefore important to point out that, since the process of photogeneration and relaxation of excitations take place at liquid-helium temperature in TSL experiments, the TSL experiments probe a quasistationary ODOS distribution. Thus, as theoretically illustrated by Arkhipov *et al.* [27],

the TSL experiments can serve as a direct optical probe of the energetic disorder of the organic semiconductor films.

In summary, the TSL technique can be used to probe the distribution of relaxed charge carriers trapped within the DOS formed as a result of energetic relaxation of charges within the DOS at low temperatures. The high-temperature wing of the classical TSL curve is an exact replica of the deeper portion of the DOS distribution, and thus, its Gaussian analysis yields the available DOS width, σ_{DOS} . Moreover, a Gaussian fit of the IR-cleansed TSL curve (σ_{TSL}) allows us to determine the ODOS width. TSL experiments conducted on pristine amorphous films of 18 low-molecular-weight organic materials commonly

used in the fabrication of OLEDs lead to the observation that the ODOS distribution formed at low temperatures is narrower than that of the DOS, with a universal ratio of $\sigma_{\text{TSL}}/\sigma_{\text{DOS}} = \sigma_{\text{ODOS}}/\sigma_{\text{DOS}} \approx 2/3$. To gain a deeper insight into this effect, we perform KMC simulations of the charge-carrier energetic relaxation process within the DOS. The KMC-simulation-based study illustrates that the spectral narrowing effect, as observed in TSL experiments, is a genuine property of carrier relaxation within the Gaussian DOS at low temperature and that spatial correlations among the energy of the hopping sites significantly reduce this narrowing effect. The results obtained within this study contribute to a better understanding of the properties of organic charge-transporting layers in both OLEDs and hybrid perovskite-based light-emitting devices. The finding of ODOS narrowing under a nonequilibrium transport regime should be considered by established hopping transport theories and might also be incorporated into device simulation tools.

ACKNOWLEDGMENTS

R.S. would like to thank Tobias Meier for discussions regarding the correlated disorder model. The authors acknowledge funding through the EU Marie Skłodowska-Curie ITN TAD*Life* grant (Grant Agreement No. 812872) and the VW Foundation. This research is also supported by the European Research Council under the ERC Grant Agreement No. 835133 (ULTRA-LUX) and by the Ministry of Education and Science of Ukraine through an external aid instrument for the fulfillment of Ukraine's commitments under the EU Framework Programme "Horizon 2020." The DFG is acknowledged for financial support through the collaborative research center TRR 146. The authors are thankful to Merck KGaA for providing HTM-2, ETM-1, and TMM-1 materials.

APPENDIX: THEORETICAL METHOD OF σ_{DOS} COMPUTATION

For morphology simulations, we adapt the Optimized Potentials for Liquid Simulations–All Atom force field (OPLS-AA) [55–57]. All Lennard-Jones parameters are taken from this force field, and we use the OPLS combination rules and a fudge factor of 0.5 for 1–4 interactions. Atomic partial charges are computed via the Merz-Kolmann method by fitting the electrostatic potential of the electron density for DFT calculations performed at the B3LYP/6-31G(d) level [58]. For parametrization of dihedral potentials the molecules are partitioned into rigid fragments [59]. By fitting fixed values of the dihedral angle between rigid fragments, molecular geometry is optimized using xTB version 6.2. [60]. The resulting potential energy surface is then fitted to the Ryckaert-Belleman polynomial, $V_{\text{RB}}(\theta) = \sum_{n=0}^5 (\cos \theta)^n$. The long-range electrostatic interactions are treated by using the

smooth-particle-mesh Ewald technique. A cutoff of 1.3 nm is used for nonbonded interactions. The equations of motion are integrated with a time step of 0.002 ps. All molecular dynamics simulations are performed in the *NPT* ensemble using the canonical velocity-rescaling thermostat [61] and the Berendsen barostat [62], as implemented in the GROMACS simulation package [63,64].

To obtain the *amorphous* morphology, systems of 243, 256, and 175 molecules for TMM-1, ETM-1, and HTM-2, respectively, are randomly inserted into the simulation box using packmol to give an isotropic cubic simulation box [65]. These systems are then simulated in the *NPT* ensemble at $T = 700$ K, $P = 1$ bar for 1 ns before cooling to 300 K during at a rate of 10 K/ns. Fast cooling freezes the isotropic orientation of the high-temperature liquid, leading to an amorphous molecular ordering.

Using the molecular dynamics trajectories, we evaluate the anion, cation, and neutral-state energies for each molecule in a morphology using a perturbative approach [66–68]. In this approach, the total energy is a sum of the gas-phase, electrostatic, and induction contributions, $E_{e,h,n} = E_{e,h,n}^{\text{gas}} + E_{e,h,n}^{\text{stat}} + E_{e,h,n}^{\text{ind}}$. To evaluate the electrostatic contribution, we calculate the Coulombic sums of distributed atomic multipoles up to the fourth order. The induction contributions to site energies are calculated self-consistently using the Thole mode [69,70], on the basis of the atomic polarizabilities and distributed multipoles obtained by using the Gaussian Distributed Multipole Analysis parametrization scheme for a cation, anion, and neutral molecule. All calculations are performed using the aperiodic Ewald summation scheme [71], as implemented in the in-house-developed VOTCA package [72].

-
- [1] W. Pasveer, J. Cottaar, C. Tanase, R. Coehoorn, P. Bobbert, P. Blom, D. De Leeuw, and M. Michels, Unified Description of Charge-Carrier Mobilities in Disordered Semiconducting Polymers, *Phys. Rev. Lett.* **94**, 206601 (2005).
 - [2] S. L. van Mensfoort, S. Vulto, R. A. Janssen, and R. Coehoorn, Hole transport in polyfluorene-based sandwich-type devices: Quantitative analysis of the role of energetic disorder, *Phys. Rev. B* **78**, 085208 (2008).
 - [3] J. Van der Holst, F. Van Oost, R. Coehoorn, and P. Bobbert, Monte Carlo study of charge transport in organic sandwich-type single-carrier devices: Effects of Coulomb interactions, *Phys. Rev. B* **83**, 085206 (2011).
 - [4] N. Tessler, Y. Preezant, N. Rappaport, and Y. Roichman, Charge transport in disordered organic materials and its relevance to thin-film devices: A tutorial review, *Adv. Mater.* **21**, 2741 (2009).
 - [5] L. J. Koster, E. Smits, V. Mihailetschi, and P. W. Blom, Device model for the operation of polymer/fullerene bulk heterojunction solar cells, *Phys. Rev. B* **72**, 085205 (2005).

- [6] H. Bässler, Charge transport in disordered organic photoconductors. A Monte Carlo simulation study, *Phys. Status Solidi B* **175**, 15 (1993).
- [7] A. Köhler and H. Bässler, *Electronic processes in organic semiconductors: An introduction* (John Wiley & Sons, Weinheim, 2015).
- [8] H. Bässler, in *Disorder Effects on Relaxational Processes*, edited by R. Richter, A. Blumen (Springer, Berlin Heidelberg New York, 1994), pp. 485.
- [9] P. Borsenberger, L. T. Pautmeier, and H. Bässler, Nondispersive-to-dispersive charge-transport transition in disordered molecular solids, *Phys. Rev. B* **46**, 12145 (1992).
- [10] P. Borsenberger, R. Richert, and H. Bässler, Dispersive and nondispersive charge transport in a molecularly doped polymer with superimposed energetic and positional disorder, *Phys. Rev. B* **47**, 4289 (1993).
- [11] S. T. Hoffmann, H. Bässler, J.-M. Koenen, M. Forster, U. Scherf, E. Scheler, P. Strohriegl, and A. Köhler, Spectral diffusion in poly (*para*-phenylene)-type polymers with different energetic disorder, *Phys. Rev. B* **81**, 115103 (2010).
- [12] S. Athanasopoulos, S. T. Hoffmann, H. Bässler, A. Köhler, and D. Beljonne, To hop or not to hop? Understanding the temperature dependence of spectral diffusion in organic semiconductors, *J. Phys. Chem. Lett.* **4**, 1694 (2013).
- [13] S. T. Hoffmann, E. Scheler, J.-M. Koenen, M. Forster, U. Scherf, P. Strohriegl, H. Bässler, and A. Köhler, Triplet energy transfer in conjugated polymers. III. An experimental assessment regarding the influence of disorder on polaronic transport, *Phys. Rev. B* **81**, 165208 (2010).
- [14] B. Ries, H. Bässler, M. Grünwald, and B. Movaghar, Monte Carlo study of relaxation and diffusion in glassy systems, *Phys. Rev. B* **37**, 5508 (1988).
- [15] R. Richert and H. Bässler, Energetic relaxation of triplet excitations in vitreous benzophenone, *Chem. Phys. Lett.* **118**, 235 (1985).
- [16] S. Van Mensfoort, V. Shabro, R. De Vries, R. Janssen, and R. Coehoorn, Hole transport in the organic small molecule material α -NPD: Evidence for the presence of correlated disorder, *J. Appl. Phys.* **107**, 113710 (2010).
- [17] S. Van Mensfoort, R. De Vries, V. Shabro, H. Loebel, R. Janssen, and R. Coehoorn, Electron transport in the organic small-molecule material BA1q—the role of correlated disorder and traps, *Org. Electron.* **11**, 1408 (2010).
- [18] D. H. Dunlap, P. E. Parris, and V. M. Kenkre, Charge-Dipole Model for the Universal Field Dependence of Mobilities in Molecularly Doped Polymers, *Phys. Rev. Lett.* **77**, 542 (1996).
- [19] S. V. Novikov, D. H. Dunlap, V. M. Kenkre, P. E. Parris, and A. V. Vannikov, Essential Role of Correlations in Governing Charge Transport in Disordered Organic Materials, *Phys. Rev. Lett.* **81**, 4472 (1998).
- [20] S. Novikov and A. Vannikov, Hopping charge transport in disordered organic materials: Where is the disorder?, *J. Phys. Chem. C* **113**, 2532 (2009).
- [21] M. Bouhassoune, S. Van Mensfoort, P. Bobbert, and R. Coehoorn, Carrier-density and field-dependent charge-carrier mobility in organic semiconductors with correlated Gaussian disorder, *Org. Electron.* **10**, 437 (2009).
- [22] A. Stankevych, A. Vakhnin, D. Andrienko, L. Paterson, J. Genoe, I. Fishchuk, H. Bässler, A. Köhler, and A. Kadashchuk, Density of States of OLED Host Materials from Thermally Stimulated Luminescence, *Phys. Rev. Appl.* **15**, 044050 (2021).
- [23] A. Kadashchuk, Y. Skryshevskii, A. Vakhnin, N. Ostapenko, V. Arkhipov, E. Emelianova, and H. Bässler, Thermally stimulated photoluminescence in disordered organic materials, *Phys. Rev. B* **63**, 115205 (2001).
- [24] A. Kadashchuk, N. Ostapenko, V. Zaika, and S. Nešpurek, Low-temperature thermoluminescence in poly (methylphenylsilylene), *Chem. Phys.* **234**, 285 (1998).
- [25] A. Kadashchuk, Y. Skryshevskii, Y. Piryatinski, A. Vakhnin, E. Emelianova, V. Arkhipov, H. Bässler, and J. Shinar, Thermally stimulated photoluminescence in poly (2, 5-dioctoxy *p*-phenylene vinylene), *J. Appl. Phys.* **91**, 5016 (2002).
- [26] A. Kadashchuk, D. Weiss, P. Borsenberger, S. Nešpurek, N. Ostapenko, and V. Zaika, The origin of thermally stimulated luminescence in neat and molecularly doped charge transport polymer systems, *Chem. Phys.* **247**, 307 (1999).
- [27] V. Arkhipov, E. Emelianova, A. Kadashchuk, and H. Bässler, Hopping model of thermally stimulated photoluminescence in disordered organic materials, *Chem. Phys.* **266**, 97 (2001).
- [28] A. Mondal, L. Paterson, J. Cho, K.-H. Lin, B. van der Zee, G.-J. A. Wetzelaer, A. Stankevych, A. Vakhnin, J.-J. Kim, and A. Kadashchuk, Molecular library of OLED host materials—evaluating the multiscale simulation workflow, *Chem. Phys. Rev.* **2**, 031304 (2021).
- [29] A. Kadashchuk, A. Vakhnin, Y. Skryshevskii, V. Arkhipov, E. Emelianova, and H. Bässler, Thermally stimulated luminescence in π -conjugated polymers containing fluorene and spirobifluorene units, *Chem. Phys.* **291**, 243 (2003).
- [30] See the Supplemental Material at <http://link.aps.org/supplemental/10.1103/PhysRevApplied.19.054007> for the full names of compounds used in this study (Note S1); more details about the fractional thermally stimulated luminescence methodology (Note S2); and determination of the DOS width, σ_{DOS} , by TSL (Note S3).
- [31] I. Tale, Trap spectroscopy by the fractional glow technique, *Phys. Status Solidi A* **66**, 65 (1981).
- [32] A. Kadashchuk, N. I. Ostapenko, Yu. A. Skryshevskii, V. I. Sugakov, and T. O. Susokolova, Clusters of dipole charge-carrier capture centers in organic crystals, *Mol. Cryst. Liq. Cryst.* **201**, 167 (1991).
- [33] V. Arkhipov, E. Emelianova, R. Schmechel, and H. Von Seggern, Thermally stimulated luminescence versus thermally stimulated current in organic semiconductors, *J. Non-Cryst. Solids* **338**, 626 (2004).
- [34] B. Schweitzer, V. Arkhipov, U. Scherf, and H. Bässler, Geminate pair recombination in a conjugated polymer, *Chem. Phys. Lett.* **313**, 57 (1999).
- [35] V. Nikitenko, D. Hertel, and H. Bässler, Dispersive geminate recombination in a conjugated polymer, *Chem. Phys. Lett.* **348**, 89 (2001).
- [36] A. Gerhard and H. Bässler, Delayed fluorescence of a poly (*p*-phenylenevinylene) derivative: Triplet–triplet annihilation versus geminate pair recombination, *J. Chem. Phys.* **117**, 7350 (2002).
- [37] C. L. Braun, S. Smirnov, S. S. Brown, and T. Scott, Picosecond transient absorption measurements of geminate

- electron-cation recombination, *J. Phys. Chem.* **95**, 5529 (1991).
- [38] A. A. Bakulin, A. Rao, V. G. Pavelyev, P. H. van Loosdrecht, M. S. Pshenichnikov, D. Niedzialek, J. Cornil, D. Beljonne, and R. H. Friend, The role of driving energy and delocalized states for charge separation in organic semiconductors, *Science* **335**, 1340 (2012).
- [39] P. de Silva and T. Van Voorhis, QM/MM study of static and dynamic energetic disorder in the emission layer of an organic light-emitting diode, *J. Phys. Chem. Lett.* **9**, 1329 (2018).
- [40] A. Lukyanov and D. Andrienko, Extracting nondispersive charge carrier mobilities of organic semiconductors from simulations of small systems, *Phys. Rev. B* **82**, 193202 (2010).
- [41] R. Saxena, T. Meier, S. Athanasopoulos, H. Bässler, and A. Köhler, Kinetic Monte Carlo Study of Triplet-Triplet Annihilation in Conjugated Luminescent Materials, *Phys. Rev. Appl.* **14**, 034050 (2020).
- [42] R. Saxena, V. Nikitenko, I. Fishchuk, Y. V. Burdakov, Y. V. Metel, J. Genoe, H. Bässler, A. Köhler, and A. Kadashchuk, Role of the reorganization energy for charge transport in disordered organic semiconductors, *Phys. Rev. B* **103**, 165202 (2021).
- [43] B. Movaghar, B. Ries, and M. Grünewald, Diffusion and relaxation of energy in disordered systems: Departure from mean-field theories, *Phys. Rev. B* **34**, 5574 (1986).
- [44] X. De Vries and R. Coehoorn, Vibrational mode contribution to the dielectric permittivity of disordered small-molecule organic semiconductors, *Phys. Rev. Mater.* **4**, 085602 (2020).
- [45] S. C. Meskers, J. Hübner, M. Oestreich, and H. Bässler, Dispersive relaxation dynamics of photoexcitations in a polyfluorene film involving energy transfer: Experiment and Monte Carlo simulations, *J. Phys. Chem. B* **105**, 9139 (2001).
- [46] S. T. Hoffmann, H. Bässler, and A. Köhler, What determines inhomogeneous broadening of electronic transitions in conjugated polymers?, *J. Phys. Chem. B* **114**, 17037 (2010).
- [47] S. T. Hoffmann, S. Athanasopoulos, D. Beljonne, H. Bässler, and A. Köhler, How do triplets and charges move in disordered organic semiconductors? A Monte Carlo study comprising the equilibrium and nonequilibrium regime, *J. Phys. Chem. C* **116**, 16371 (2012).
- [48] F. B. Dias, T. J. Penfold, and A. P. Monkman, Photophysics of thermally activated delayed fluorescence molecules, *Methods Appl. Fluoresc.* **5**, 012001 (2017).
- [49] D. Sun, R. Saxena, X. Fan, S. Athanasopoulos, E. Duda, M. Zhang, S. Bagnich, X. Zhang, E. Zysman-Colman, and A. Köhler, Regiochemistry of donor dendrons controls the performance of thermally activated delayed fluorescence dendrimer emitters for high efficiency solution-processed organic light-emitting diodes, *Adv. Sci.* **9**, 2201470 (2022).
- [50] Y. Liu, K. Zojer, B. Lassen, J. Kjelstrup-Hansen, H.-G. Rubahn, and M. Madsen, Role of the charge-transfer state in reduced Langevin recombination in organic solar cells: A theoretical study, *J. Phys. Chem. C* **119**, 26588 (2015).
- [51] F.-J. Kahle, A. Rudnick, H. Bässler, and A. Köhler, How to interpret absorption and fluorescence spectra of charge transfer states in an organic solar cell, *Mater. Horiz.* **5**, 837 (2018).
- [52] T. Upreti, S. Wilken, H. Zhang, and M. Kemerink, Slow relaxation of photogenerated charge carriers boosts open-circuit voltage of organic solar cells, *J. Phys. Chem. Lett.* **12**, 9874 (2021).
- [53] A. Melianas, N. Felekidis, Y. Puttison, S. C. Meskers, O. Inganäs, W. M. Chen, and M. Kemerink, Nonequilibrium site distribution governs charge-transfer electroluminescence at disordered organic heterointerfaces, *Proc. Natl. Acad. Sci. U. S. A.* **116**, 23416 (2019).
- [54] F. J. Kahle, A. Rudnick, S. Wedler, R. Saxena, R. Ammenhäuser, U. Scherf, S. Bagnich, H. Bässler, and A. Köhler, Static and dynamic disorder of charge transfer states probed by optical spectroscopy, *Adv. Energy Mater.* **12**, 2103063 (2022).
- [55] W. L. Jorgensen and J. Tirado-Rives, Potential energy functions for atomic-level simulations of water and organic and biomolecular systems, *Proc. Natl. Acad. Sci. U. S. A.* **102**, 6665 (2005).
- [56] W. L. Jorgensen and J. Tirado-Rives, The OPLS [optimized potentials for liquid simulations] potential functions for proteins, energy minimizations for crystals of cyclic peptides and crambin, *J. Am. Chem. Soc.* **110**, 1657 (1988).
- [57] W. L. Jorgensen, D. S. Maxwell, and J. Tirado-Rives, Development and testing of the OPLS all-atom force field on conformational energetics and properties of organic liquids, *J. Am. Chem. Soc.* **118**, 11225 (1996).
- [58] U. C. Singh and P. A. Kollmann, An approach to computing electrostatic charges for molecules, *J. Comput. Chem.* **5**, 129 (1984).
- [59] C. Poelking, E. Cho, A. Malafeev, V. Ivanov, K. Kremer, C. Risko, J.-L. Brédas, and D. Andrienko, Characterization of charge-carrier transport in semicrystalline polymers: Electronic couplings, site energies, and charge-carrier dynamics in poly (bithiophene-*alt*-thienothiophene)[PBTTT], *J. Phys. Chem. C* **117**, 1633 (2013).
- [60] C. Bannwarth, E. Caldeweyher, S. Ehlert, A. Hansen, P. Pracht, J. Seibert, S. Spicher, and S. Grimme, Extended tight-binding quantum chemistry methods, *WIREs Comput. Mol. Sci.* **11**, e01493 (2020).
- [61] G. Bussi, D. Donadio, and M. Parrinello, Canonical sampling through velocity rescaling, *J. Chem. Phys.* **126**, 014101 (2007).
- [62] H. J. Berendsen, J. v. Postma, W. F. van Gunsteren, A. DiNola, and J. R. Haak, Molecular dynamics with coupling to an external bath, *J. Chem. Phys.* **81**, 3684 (1984).
- [63] B. Hess, C. Kutzner, D. Van Der Spoel, and E. Lindahl, GROMACS 4: Algorithms for highly efficient, load-balanced, and scalable molecular simulation, *J. Chem. Theory Comput.* **4**, 435 (2008).
- [64] S. Pronk, S. Páll, R. Schulz, P. Larsson, P. Bjelkmar, R. Apostolov, M. R. Shirts, J. C. Smith, P. M. Kasson, D. van der Spoel, B. Hess, and E. Lindahl, GROMACS 4.5: A high-throughput and highly parallel open source molecular simulation toolkit, *Bioinformatics* **29**, 845 (2013).
- [65] L. Martínez, R. Andrade, E. G. Birgin, and J. M. Martínez Packmol: A package for building initial configurations for molecular dynamics simulations, *J. Comput. Chem.* **30**, 2157 (2009).

- [66] A. Stone, *The theory of intermolecular forces* (OUP oxford, Oxford, 2013).
- [67] G. D'Avino, L. Muccioli, F. Castet, C. Poelking, D. Andrienko, Z. G. Soos, J. Cornil, and D. Beljonne, Electrostatic phenomena in organic semiconductors: Fundamentals and implications for photovoltaics, *J. Phys.: Condens. Matter* **28**, 433002 (2016).
- [68] C. Poelking and D. Andrienko, Long-range embedding of molecular ions and excitations in a polarizable molecular environment, *J. Chem. Theory Comput.* **12**, 4516 (2016).
- [69] B. T. Thole, Molecular polarizabilities calculated with a modified dipole interaction, *Chem. Phys.* **59**, 341 (1981).
- [70] P. T. Van Duijnen and M. Swart, Molecular and atomic polarizabilities: Thole's model revisited, *J. Phys. Chem. A* **102**, 2399 (1998).
- [71] A. J. Stone, Distributed multipole analysis: Stability for large basis sets, *J. Chem. Theory Comput.* **1**, 1128 (2005).
- [72] V. Rühle, A. Lukyanov, F. May, M. Schrader, T. Vehoff, J. Kirkpatrick, B. Baumeier, and D. Andrienko, Microscopic simulations of charge transport in disordered organic semiconductors, *J. Chem. Theory Comput.* **7**, 3335 (2011).